Bull. Astr. Soc. India (2011) **39**, 547–562

A low-frequency study of two asymmetric large radio galaxies

A. Pirya,[1*] S. Nandi,[1] D. J. Saikia[2] and M. Singh[1]

[1]*Aryabhatta Research Institute of Observational Sciences (ARIES), Manora Peak, Nainital, 263 129, India*
[2]*National Centre for Radio Astrophysics, TIFR, Pune University Campus, Post Bag 3, Pune 411 007, India*

Received 2011 December 27; accepted 2012 January 04

Abstract. We present the results of multifrequency observations of two asymmetric, Mpc-scale radio sources with the Giant Metrewave Radio Telescope (GMRT) and the Very Large Array (VLA). The radio luminosity of these two sources, J1211+743 and J1918+742, are in the Fanaroff-Riley class II (FRII) range, but have diffuse radio components on one side of the galaxy while the opposite component appears edge-brightened with a prominent hot-spot. Although the absence of a hot-spot is reminiscent of FRI radio galaxies, suggesting a hybrid morphology, the radio jet facing the diffuse lobe in J1211+743 is similar to those in FRII radio sources, and it is important to consider these aspects as well while classifying these sources in the FR scheme. The observed asymmetries in these Mpc-scale sources are likely to be largely intrinsic rather than being due to the effects of orientation and relativistic motion. The formation of a diffuse lobe facing the radio jet in J1211+743 is possibly due to the jet being highly dissipative. The low-frequency spectral indices of the lobes are in the range of approximately −0.8 to −1, while at the outer edges these vary from approximately −0.65 to −1.05 suggesting steep injection spectral indices, which need to be examined further from observations at even lower frequencies by telescopes such as the LOw Frequency ARray (LOFAR).

Keywords : galaxies: active – galaxies: jets – galaxies: nuclei – radio continuum: galaxies – galaxies: individual: J1211+743 – galaxies: individual: J1918+742

1. Introduction

Studies of asymmetries in luminous extragalactic radio sources have provided valuable insights towards understanding a number of important aspects of these sources. While the correlation

*email: akashpirya@gmail.com (AP); sumana@aries.res.in (SN), djs@ncra.tifr.res.in (DJS) and msingh@aries.res.in (MS)

of depolarization asymmetry with jet sidedness (Laing 1988; Garrington et al. 1988) has established the importance of orientation in understanding jet asymmetry, structural asymmetries of the oppositely-directed components have also been used by a number of authors over the years (e.g. Gilbert et al. 2004; Gopal-Krishna & Wiita 2005; Mullin, Riley & Hardcastle 2008, and references therein) to test the orientation-dependent unified schemes for active galaxies since the early work by Kapahi & Saikia (1982). In addition to the effects of orientation, environmental asymmetries have also been seen to play an important role. McCarthy, van Breugel & Kapahi (1991) showed the presence of more extended emission line gas on the side of the source with the shorter component in radio galaxies. In a sample of radio sources with or without radio jets, the shorter component appears to depolarize faster (e.g. Pedelty et al. 1989) possibly due to interaction with the gas clouds, two of the most extreme examples being 3C254 (Thomasson, Saikia & Muxlow 2006) and 3C459 (Thomasson, Saikia & Muxlow 2003). Radio structural asymmetries have been used to probe intrinsic and environmental asymmetries on different scales ranging from the compact steep-spectrum (CSS) and giga-Hertz peaked spectrum (GPS) objects (e.g. Saikia et al. 1995, 2001) to the giant radio sources (GRS) with projected sizes of over a Mpc (e.g. Subrahmanyan et al. 2008). The possibility of the environment playing an important role in the observed asymmetries is consistent with a slow velocity of propagation of the jet head suggested by Scheuer (1995; see also O'Dea et al. 2009; Konar et al. 2009). Structural asymmetries of the oppositely-directed components have been used to probe the 'flip-flop' model for radio sources, where energy supply from the nucleus is one-sided at a time, but the source appears reasonably symmetric averaged over its life time (e.g. Saikia & Wiita 1982; Rudnick & Edgar 1984).

Effects of orientation and relativistic motion on the spectra of the hot-spots or lobes have also been studied (see Garrington, Conway & Leahy 1991; Dennett-Thorpe et al. 1997, 1999; Ishwara-Chandra & Saikia 2000; Mullin et al. 2008). While the high-brightness regions appear to have flatter spectra on the side facing the jet, consistent with mild relativistic beaming, the spectral asymmetries of the extended regions appear to depend on the lobe length (Dennett-Thorpe et al. 1999). Liu & Pooley (1991a,b) found that for a sample consisting mostly of galaxies, the more depolarized component has a steeper radio spectrum. Ishwara-Chandra et al. (2001) examined the dependence of the Liu-Pooley relationship on size, optical identification and redshift and found it to be significantly stronger for smaller sources, and similar for both radio galaxies and quasars. In addition to Doppler effects, there also appears to be intrinsic differences between the oppositely-directed components.

While most structural asymmetries can be understood by taking into account the effects of both an asymmetric, inhomogeneous environment and relativistic motion (e.g. Jeyakumar et al. 2005; see Gaibler, Khochfar & Krause 2011 for results of recent simulations of jet-disk interaction), MERLIN (Multi-Element Radio Linked Interferometer Network) and VLA (Very Large Array) observations of one-sided radio sources revealed a possible class of weak-cored, one-sided sources which were difficult to understand in the simple relativistic beaming scenario (e.g. Saikia et al. 1989, 1990). Saikia et al. (1996) also highlighted the very asymmetric radio galaxy B0500+630, where one component had an FRII structure (Fanaroff & Riley 1974) while the other one appeared to be of FRI type. It was difficult to understand its asymmetries in the relativistic beaming scenario. Gopal-Krishna & Wiita (2000) examined the detailed structure of

Table 1. Properties of the two sources.

Source name	RA (J2000) hh mm ss.ss	Dec (J2000) dd mm ss.s	z	Refs.	LAS $''$	size kpc	log $P_t^{1.4}$ W/Hz
(1)	(2)	(3)	(4)	(5)	(6)	(7)	(8)
J1211+743	12 11 59.03	74 19 04.7	0.1070	MO79	437	846	25.17
J1918+742	19 18 34.81	74 15 04.9	0.1940	L01b;P	397	1266	25.63

References: MO79: Miley & Osterbrock 1979; L01b: Lara et al. 2001b; P: Present work (the position of the optical galaxy was estimated from the Digital Sky Survey image). For J1211+743 and J1918+742, one arcsec corresponds to 1.935 and 3.190 kpc respectively.

a large number of sources and identified several with FRI and FRII structures on opposite sides, and christened these as HYMORS (HYbrid MOrphology Radio Sources). They inferred that such sources indicate that the FR dichotomy is due to interaction with the external medium rather than differences in the central engine.

From a representative sample of ∼40 radio galaxies selected from the B2 sample, Parma et al. (1999) classified the spectral index variation along the oppositely-directed components into three types. Those where the spectral index increases from the core outwards, which is typical of the buoyant plumes of large FRI sources like 3C31 (Laing et al. 2008), were called type 1, while those where the spectral index increases from the outer edges of the components towards the core were called type 2. Type 2 sources could be of either FRI or FRII type. In addition, a small fraction of ∼10 per cent showed no significant variation along the source axis. These were christened as type 3, and non-variation of spectral index along the components was suggested to be due to particle re-acceleration. In a recent detailed study of lobe-like FRI radio galaxies which all had jets similar to the ones in FRI sources embedded within their lobes, Laing et al. (2011) noted similarities in the spectral index variation with FRII sources. While the jets and 'caps' at the edges of the lobes tend to have flatter spectra with spectral indices in the range of −0.5–0.7, the outer edges of the lobes and plasma closer to the core tend to have significantly steeper spectra. However, sometimes there is very little variation over most of the lobe emission as seen in the images of B0755+37 and M84 by Laing et al. (2011), the former being classified as type 3 by Parma et al. (1999).

2. J1211+743 and J1918+742

To further explore the asymmetries and low-frequency spectra and structure of Mpc-scale radio galaxies, we present the results of Giant Metrewave Radio Telescope (GMRT) and VLA observations of two large, asymmetric radio sources, J1211+743 and J1918+742, which have an FRII-like component containing a hot-spot on one side and a diffuse lobe on the opposite side. In the case of J1211+743 a well-collimated radio jet faces the diffuse lobe. These two sources are both associated with galaxies and have been selected from the sample of large sources compiled by Lara et al. (2001a). Some of their basic features are summarised in Table 1, which is arranged as follows. Column 1: Source name; columns 2 and 3: Right Ascension and Declination in J2000 co-ordinates; column 4: redshift of the source; column 5: references for the position and redshift

of the host galaxy; column 6: the largest angular size in arcsec; column 7: linear size in kpc for a Universe with H_o=71 km s^{-1} Mpc^{-1}, Ω_m=0.27, Ω_{vac}=0.73 (Spergel et al. 2003); column 8: the log of the luminosity (in W/Hz) at 1.4 GHz.

2.1 Notes on the sources

J1211+743 (4CT 74.17.01): The radio galaxy J1211+743 with a projected linear size of ∼846 kpc, has been observed by a number of authors over the years (e.g. Rudnick & Owen 1977; van Breugel & Willis 1981; Fanti et al. 1983; Jägers 1986; Zhao et al. 1989; Schoenmakers et al. 2000, 2001; Lara et al. 2001b). Rudnick & Owen (1977) identified the source with the south-west member of a pair of bright galaxies in Abell 1500. The nearby companion galaxy is ∼7.5 arcsec away (Lara et al. 2001b). The radio structure shows a prominent hot-spot in the southern component while the northern component appears as a diffuse lobe (Figs. 1 and 2). The maximum value of the peak brightness ratio in the oppositely-directed components is ∼6.5. The source has a wiggling jet towards the north with the magnetic field lines along the direction of the jet (van Breugel & Willis 1981). A weak counter-jet has been reported by Lara et al. (2001a).

J1918+742: The giant radio galaxy J1918+742 with a projected linear size of ∼1.3 Mpc (Figs. 1 and 3) has been imaged earlier at 1.4 and 4.9 GHz with the VLA by Lara et al. (2001a,b). It has a prominent hot-spot on the western component while the eastern component is diffuse without a significant hot-spot. The maximum ratio of the peaks of emission in the oppositely-directed components is ∼13.

The observations and analyses of these two sources are described briefly in Section 3, while the observational results are presented in Section 4. These results are discussed in Section 5, and summarised in Section 6.

3. Observations and analyses

The GMRT and VLA observations were made in the standard fashion, with the target source observations being interspersed by the observations of the phase calibrators. The observing log for all the observations is shown in Table 2 which is arranged as follows. Columns 1 and 2: name of the source and the telescope; column 3: the frequency of the observations in MHz; column 4: phase calibrators used for the different observations; column 5: the dates of the observations. The primary flux density and bandpass calibrators were 3C48, 3C147 and 3C286. The flux densities at frequencies below 408 MHz have been extrapolated using the parameters given by Baars et al. (1977), while at higher frequencies these are in the Baars et al. (1977) scale. At low frequencies, the assumed flux densities of 3C48 are 50.72 and 43.41 Jy at 239 and 332 MHz respectively, while for 3C286 the corresponding values are 28.07 and 25.96 Jy respectively. 3C147 was observed at 333 MHz and its flux density was assumed to be 52.69 Jy. The total observing time on each source is about 8 hr for the GMRT observations and ∼10 min for the VLA observations. All the data were analyzed in the standard fashion using the NRAO `AIPS` package.

Table 2. Observing log.

Source	Telescope	Obs. freq. MHz	Phase calibrator	Obs. date
(1)	(2)	(3)	(4)	(5)
J1211+743	GMRT	239	J0834+555 J1459+716	2008 Dec 02
	GMRT	333	J0834+555 J1459+716	2008 Dec 30
	GMRT	607	J0834+555 J1459+716	2008 Dec 02
	VLA[a]	4885	J1048+717	1997 Jul 27
J1918+742	GMRT	239	J1459+716 J2350+646	2008 Dec 27
	GMRT	332	J1459+716	2009 Mar 10
	GMRT	607	J1927+739	2009 Dec 27

[a] archival data from the VLA

The low-frequency GMRT data were significantly affected by radio frequency interference (RFI), and these data were flagged using different tasks, such as `UVFLG`, `TVFLG` and `SPFLG` available in `AIPS`. For the GMRT observations, we initially calibrated the data for one channel, and then applied bandpass calibration, using the task `BPASS` for calculating the gains of all other channels. Channel averaging was done to obtain the continuum data sets. These continuum data sets were imaged and CLEANed using multiple facets for the different low-frequency GMRT observations using the task `IMAGR`. All the data were self calibrated using a clean component model in the task `CALIB` to produce the final images, which were then corrected for the primary beam response.

4. Observational results

The GMRT full-resolution images of the J1211+743 and J1918+742 with angular resolutions of 7.6×5.1 arcsec^2 along position angle (PA) 32° and 6.6×6.1 arcsec^2 along PA 42° are presented in Fig. 1. The peak brightness of the northern lobe of J1211+743 is 3 mJy/beam compared with 15 mJy/beam for the southern lobe. The corresponding values for the western and eastern lobes of J1918+742 are 69 and 7 mJy/beam respectively. The angular sizes of the lobes are smaller than the largest scale structures visible to the GMRT (http://gmrt.ncra.tifr.res.in), and we have checked that short-spacing data were available to image these sources reliably. To study the spectra of the lobes over at least a factor of $\gtrsim$5 in frequency the images of J1211+743 have been convolved with an angular resolution of 18 arcsec, similar to the coarsest resolution of our images. The images at frequencies >300 MHz were initially made by tapering the data and then convolving these to a common resolution. For J1918+742 we have chosen an angular resolution of 45 arcsec so that these are all similar to the NRAO VLA Sky Survey (NVSS; Condon et al. 1998) image. However, we also imaged the GMRT low-frequency data of J1918+742 with an angular resolution of 16 arcsec over a smaller frequency range to check for consistency of the results. The 18-arcsec

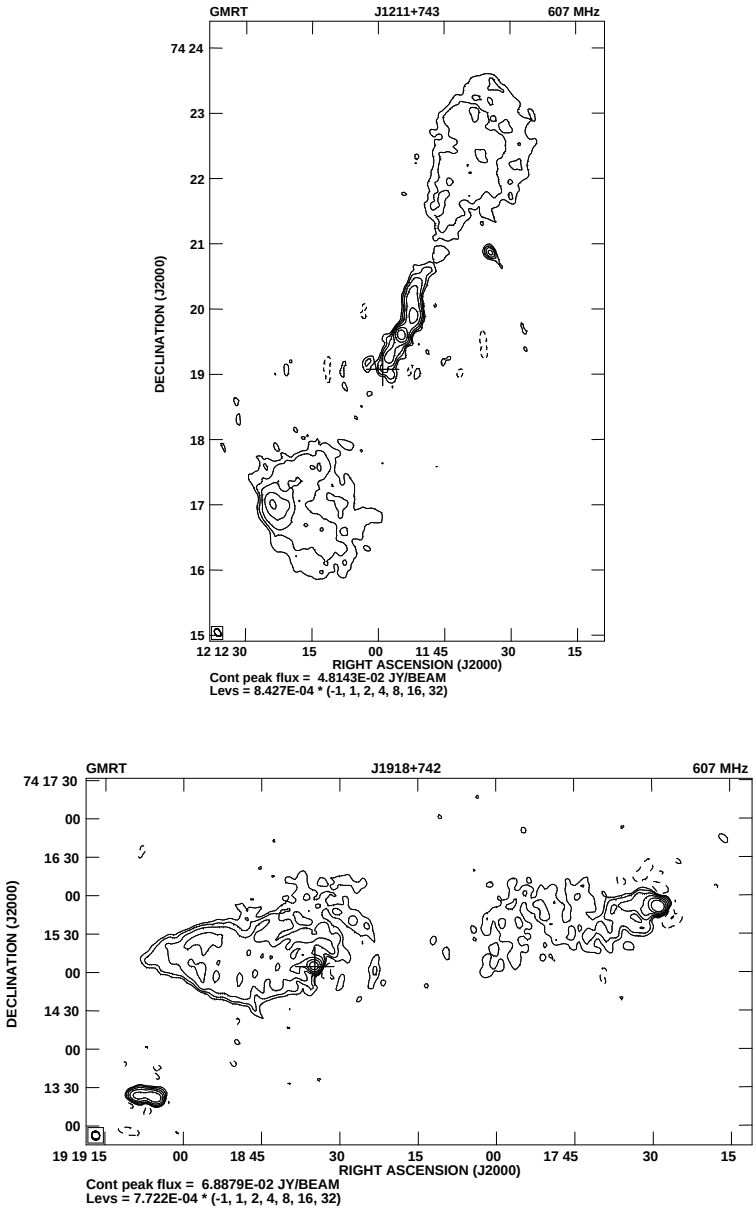

Figure 1. GMRT full-resolution images of J1211+743 and J1918+742 at 607 MHz with angular resolutions of ∼6 arcsec, which illustrate the diffuse lobes without a prominent hot-spot, reminiscent of FRI lobes, on one side, and an edge-brightened lobe with a hot-spot on the opposite side. The + sign denotes the position of the optical galaxy.

resolution images of J1211+743 and the 45-arcsec resolution images of J1918+742 are shown in Figs. 2 and 3 respectively, while the observational parameters and some of the observed properties are tabulated in Table 3 which is arranged as follows. Column 1: Frequency of the observations in units of MHz, where G or V indicates either GMRT or VLA observations respectively; column 2: the resolution of the image in arcsec; column 3: the rms noise in units of mJy/beam; columns 4, 5: peak and integrated flux density of the entire source in units of mJy/beam and mJy respectively. The flux densities for each source and its components at different frequencies have been estimated over similar areas. Columns 6, 9, 11: components designations, where N, W, C, S, E denote northern, western, core, southern and eastern components respectively; columns 7 and 8, 12 and 13: peak and total flux densities of each component in units of mJy/beam and mJy respectively. For the cores, only the peak brightness is quoted in column 10, to minimise contamination by extended emission in their vicinity. The total flux densities have been estimated by specifying an area around the components. The components refer to the entire lobe emission, but excluding the radio jet in J1211+743 whose flux densities are listed at the bottom of Table 3. We examined the change in flux density by varying the area around the components, and find that the typical errors in the flux densities, including calibration errors, are ∼14 per cent at ∼235 and 325 MHz, ∼10 per cent at 610 MHz and ∼5 per cent at higher frequencies (cf. Konar et al. 2008; Nandi et al. 2010). The integrated spectra of the sources, as well as the spectra of the different components by combining the results of our observations with existing data in the literature are shown in the left panels of Figs. 4 and 5. We have fitted the spectra using both a linear least squares fit as well as a parabolic fit, and find the linear fits to be better.

5. Results and discussions

5.1 Component brightness asymmetry

Although the radio luminosity of these sources is in the FRII category, one of the components in these two sources is diffuse with no significant hot-spot at its outer edge. Although the diffuse lobes are reminiscent of those in FRI radio galaxies, the radio jet in J1211+743 is well-collimated (see Fig. 1) with the magnetic field lines following the bends in the jet (van Breugel & Willis 1981). This is similar to what is usually seen in jets in FRII radio sources (e.g. Bridle & Perley 1984), suggesting that one needs to examine the jet and magnetic field structures as well as the structure of the lobes before classifying these sources as being of hybrid FRI/FRII morphology.

Asymmetries in the peak brightness of the lobes could be due to either relativistic motion of the hot-spots or intrinsic asymmetries in the sources or their environments. However, since these are all large Mpc-scale sources associated with galaxies, relativistic motion is not likely to be a dominant factor. The fraction of emission from the core at an emitted frequency of 8 GHz, which is a statistical indicator of orientation of the jet axis to the line of sight is ∼0.08 and 0.05 for J1211+743 and J1918+742 respectively. These values overlap with the distribution for quasars and are significantly higher than the median value of 0.002 for 3CRR radio galaxies (Saikia & Kulkarni 1994). We therefore assume that these are close to the dividing line between galaxies and quasars and adopt an inclination angle of 45° (Barthel 1989). Most luminous radio galaxies

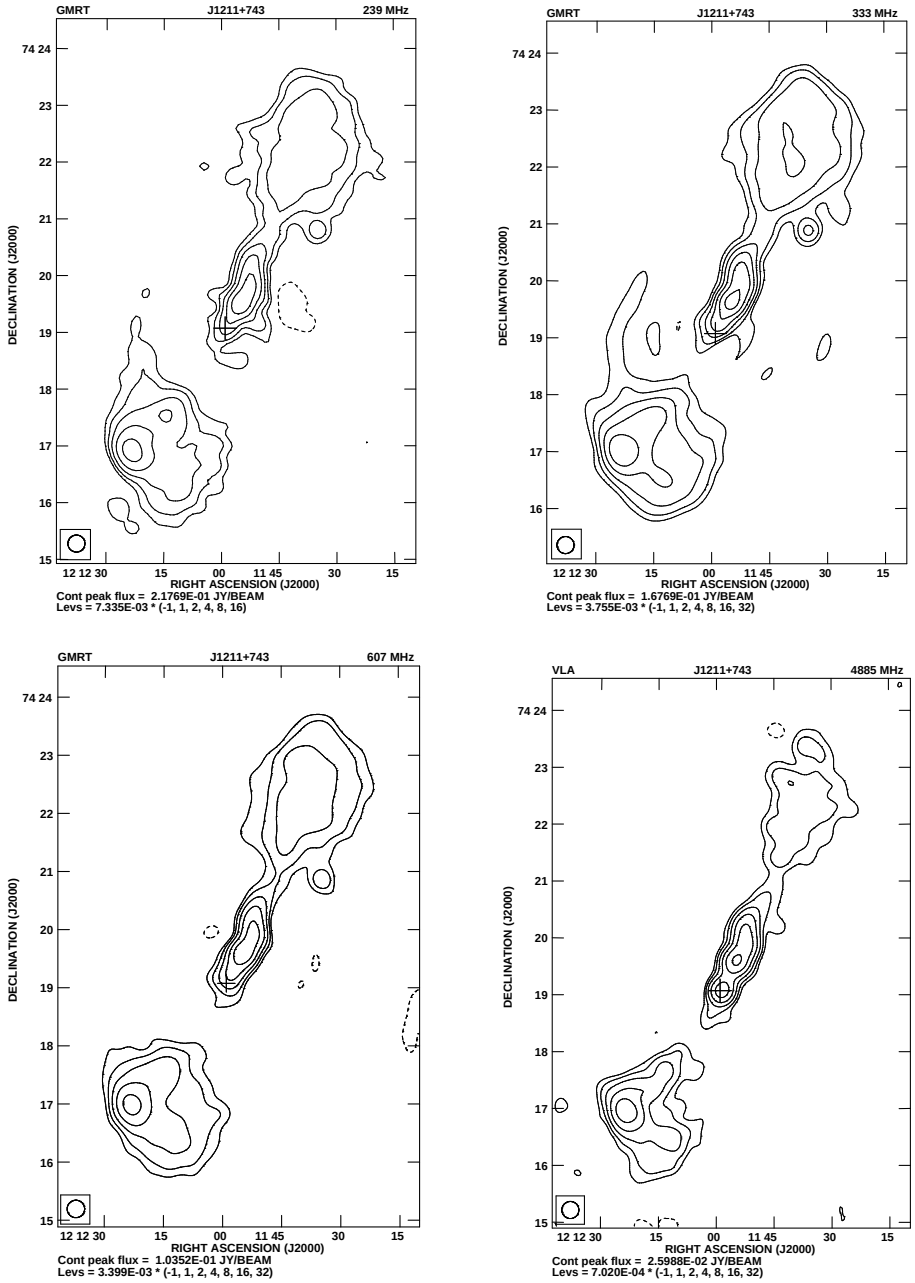

Figure 2. GMRT low-frequency images of J1211+743 at 239, 333, 607 MHz and the VLA high-frequency image at 4885 MHz with an angular resolution of 18 arcsec. The + sign indicates the position of the optical galaxy.

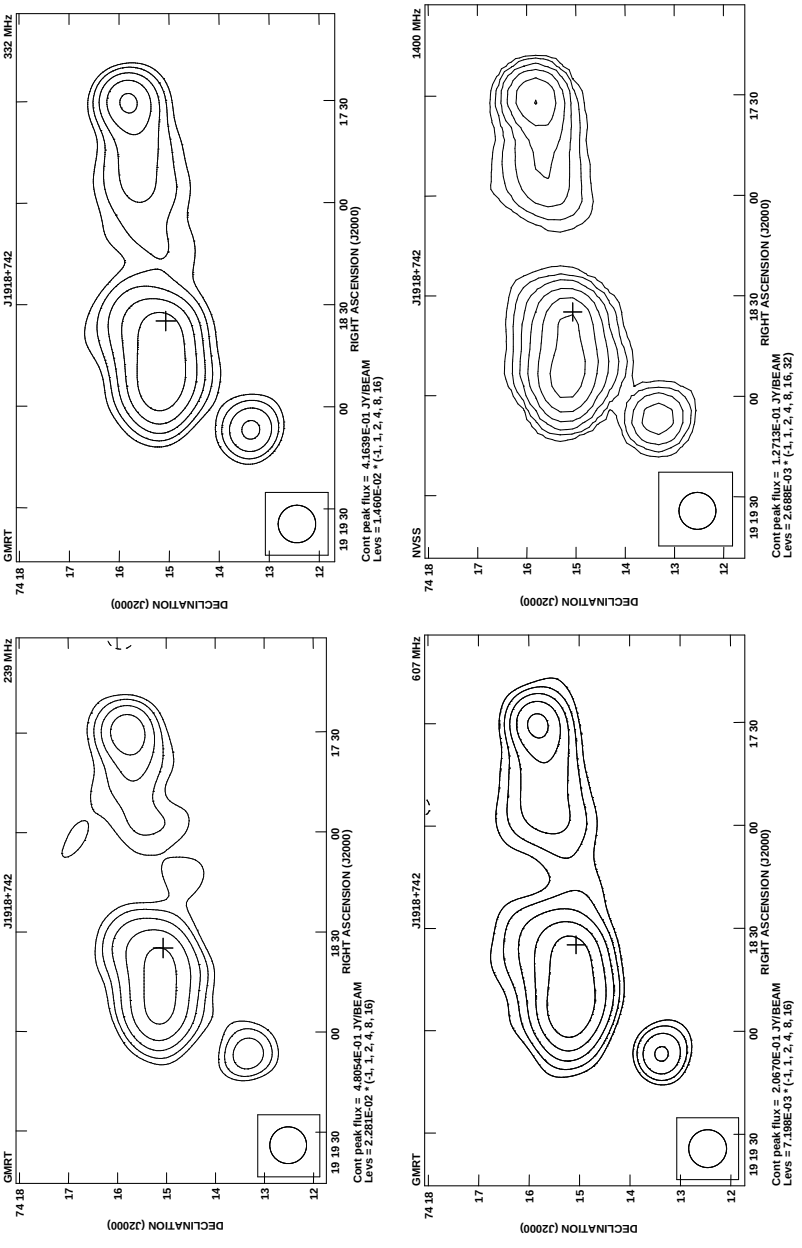

Figure 3. GMRT low-frequency images of J1918+742 at 239, 332 and 607 MHz, and the VLA NVSS image at 1400 MHz. The resolution of these images is 45 arcsec. The + sign indicates the position of the optical galaxy.

Table 3. The observational parameters and observed properties of the sources.

Freq.	res.	rms	S_p	S_I	Cmp.	S_p	S_t	Cmp.	S_p	Cmp.	S_p	S_t
MHz	$''$	mJy	mJy	mJy		mJy	mJy		mJy		mJy	mJy
		/b	/b			/b			/b		/b	
(1)	(2)	(3)	(4)	(5)	(6)	(7)	(8)	(9)	(10)	(11)	(12)	(13)
J1211+743*												
G239	18	1.48	218	3681	N	49	1359	C	≤32	S	163	1533
G333	18	0.81	168	2507	N	33	877	C	≤16	S	118	1033
G607	18	0.79	104	1420	N	23	530	C	11	S	73	595
V4885	18	0.27	26	234	N	3	49	C	13	S	18	96
J1918+742												
G239	16	1.81	194	2500	W	194	675	C	≤70	E	115	1760
	45	5.98	481	2575	W	311	691	C		E	481	1843
G332	16	0.76	175	2240	W	175	627	C	≤64	E	114	1570
	45	3.07	416	2308	W	267	661	C		E	416	1648
G607	16	0.69	102	1089	W	102	319	C	46	E	61	608
	45	1.80	207	1176	W	140	348	C		E	207	741
V1400	45	0.89	127	575	W	88	175	C		E	127	400

* The peak and total flux densities of the jet from the images with an angular resolution of 18 arcsec are as follows. 239 MHz: 218 mJy/b and 819 mJy; 333 MHz: 168 mJy/b and 549 mJy; 607 MHz: 104 mJy/b and 296 mJy; 4885 MHz: 26 mJy/b and 77 mJy

are likely to have small values of speeds of advancement of $\lesssim 0.1c$ (e.g. Scheuer 1995; see also O'Dea et al. 2009; Konar et al. 2009). For J1211+743, Machalski et al. (2007) estimated an advancement speed of the head of $0.009c$ from their modelling of the dynamics of the source. The maximum values of the peak brightness ratio on opposite sides of the nucleus are ~6.5 and 13 for the two sources respectively (see Table 3). For an inclination angle, ϕ, of 45°, an advancement speed (βc) of $0.1c$, and a spectral index, $\alpha \sim -1$, (defined as $S \propto \nu^{\alpha}$), the expected brightness ratio, $\{(1+\beta\cos\phi)/(1-\beta\cos\phi)\}^{(2-\alpha)}$ (e.g. Blandford & Königl 1979) is only ~1.5. This is significantly smaller than the observed values suggesting intrinsic asymmetries in the sources. In the case of J1211+743, the diffuse lobe is on the side of the radio jet, which is also contrary to what would be expected in the relativistic beaming scenario. The ratio of the peak brightness in the jet of J1211+743 to 3σ, where σ is the rms noise in the counter-jet side in the GMRT 607-MHz image, is $\gtrsim 50$. This implies that the jet velocity would have to be $\gtrsim 0.8c$ for $\phi \sim 45°$ and $\alpha \sim -0.7$, if the asymmetry is due to bulk relativistic motion. Considering the overall structure of the source, the observed jet asymmetry could be largely due to an asymmetric dissipation of energy on the opposite sides, leading to the formation of a diffuse lobe without a prominent hot-spot on the jet side. Such a possibility has been suggested earlier for a number of radio jets in quasars such as in B1004+13, B1857+566 and 3C280.1 where the radio jet points towards a lobe without a

significant hot-spot, while the edge-brightened component on the opposite side has a prominent hot-spot (e.g. Saikia 1984; see also Gopal-Krishna, Wiita & Hooda 1996).

5.2 Radio spectra

The integrated radio spectra and those of the components for J1211+743 and J1918+742 are shown in Figs. 4 and 5 respectively. For J1211+743, the integrated spectral index is -0.83 ± 0.02, while the values of α for the northern, southern and jet components are -1.02 ± 0.03, -0.88 ± 0.02 and -0.71 ± 0.03 respectively. The integrated spectral index for J1918+742 is -0.97 ± 0.04, while the spectral indices for the western and eastern components are -0.77 ± 0.05 and -1.05 ± 0.06 respectively. We attempted both a straight-line and parabolic fit, and find that straight line fits are consistent with the available data, although for J1211+743 the 10.7 GHz measurements by Schoenmakers et al. (2000, 2001) suggest a steepening of the spectra of the lobes. As expected, both the components with a hot-spot have flatter spectral indices than the components on the opposite side.

We also examine the variation in spectral index across the components for the two sources. To get reliable values of spectral index profiles we determined the spectral indices from measurements at a minimum of four frequencies differing by a factor of at least ∼5. High-frequency measurements at greater than a few GHz were available only for J1211+743. As discussed earlier, the images of J1211+743 were made with an angular resolution of 18 arcsec, similar to the lowest resolution of our observations. For J1918+742 the low-frequency GMRT images were convolved with a resolution of 45 arcsec, the resolution of the NVSS image, since higher frequency data were not available. For each source we estimated the spectral indices in identical areas with significant flux density at all the frequencies, and separated by about a beamwidth. The images were aligned, rotated to be along the east-west direction and regridded so that the flux densities in each area of a source were estimated in identical boxes at the different frequencies using the `AIPS` task `IMEAN`. We have followed a similar procedure as in our earlier studies (e.g. Jamrozy et al. 2008; Konar et al. 2008; Nandi et al. 2010). The right panels of Figs. 4 and 5 show the spectral index variation across the components. Distances have been measured from either the hot-spot or the centre of the first strip at the outer edge of the component.

For the radio galaxy J1211+743, there have been a couple of attempts in the past to examine the variation of spectral index across the source from observations at a limited number of frequencies. Jägers (1986) found the two-point spectral index α_{609}^{1415} to exhibit a large steepening with distance from the hot-spot for the southern component with α varying from approximately -0.7 to -2.0 over a distance of ∼2 arcmin (∼230 kpc), a relatively smaller gradient for the northern diffuse lobe with α varying from approximately -0.8 to -1.2 over a similar length scale, and the jet region to show very little variation along its length with α approximately -0.7. Schoenmakers et al. (2000, 2001) also find a flatter spectrum region in the vicinity of the radio jet in both the spectral index profiles α_{354}^{10450} and α_{354}^{1400} with $\alpha\sim-0.7$ to -0.65. However their profiles α_{354}^{10450} and α_{354}^{1400} for both the lobes are very different from each other. For example, α_{354}^{10450} appears to flatten farther away from the edge and towards the core for the northern lobe and exhibits no

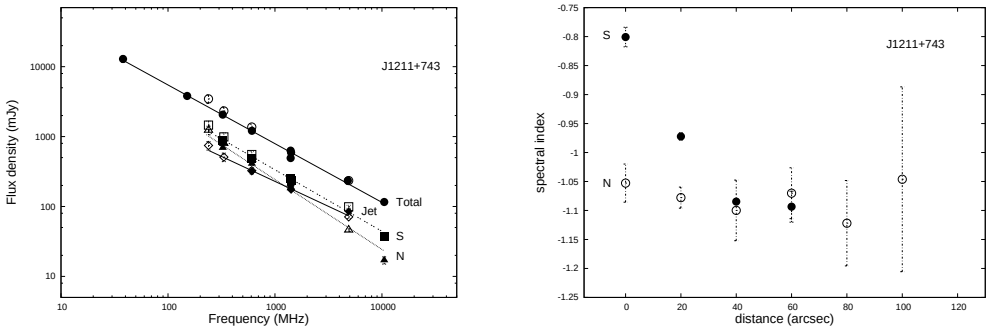

Figure 4. Left panel: the spectra of the J1211+743 and its components. The values have been taken from the following references: 38 MHz, Rees (1990); 151 MHz, Hales et al. (1991); 325, 4850 and 10500 MHz, Schoenmakers et al. (2000, 2001); 608.5, 1415 and 4885 MHz, van Breugel & Willis (1981); 1400 MHz, NVSS survey; 1400 MHz, White & Becker (1992); 239, 333, 607 and 4885 MHz, from this paper. Right panel: The spectral index profiles for the northern and southern components with an angular resolution of 18 arcsec, using our measurements at 239, 333, 607 and 4865 MHz. For J1211+743, one arcsec corresponds to 1.935 kpc.

significant variation in the southern lobe, while α_{354}^{1400} appears to steepen with distance from the edge for both the lobes. Over the limited distances that we have determined the profiles for α_{239}^{4885}, which have been estimated by a least-squares fit to flux densities at four frequencies in regions of high signal to noise ratio, the trends are broadly consistent with those of Jägers (1986). The southern lobe exhibits a significant steepening with α varying from approximately -0.8 to -1.1 over a distance of $\sim$50 arcsec ($\sim$100 kpc) while the variation in the northern lobe is very marginal over a similar distance. For the radio galaxy J1918+742, where the eastern component is diffuse with no prominent hot-spot, and the optical galaxy/radio core is shifted significantly towards the east, the spectra of both components appear to steepen with distance from the outer edge of the components. Here the spectral indices α_{239}^{1400} have been determined from images with an angular resolution of 45 arcsec, and the spectral index varies from approximately -0.65 to -1.05 over $\sim$120 arcsec ($\sim$380 kpc) for the western lobe and from approximately -0.75 to -0.95 over $\sim$80 arcsec ($\sim$255 kpc). The trend is consistent with what is normally observed in most FRII radio galaxies.

It is relevant to note that the frequency range used for estimating the integrated spectral indices is larger than that of the components, with total flux density measurements being available at 38 MHz. Spectral indices at low frequencies, especially at the outer edges of the lobes, reflect the injection spectra, and our values are consistent with earlier estimates in the literature. For comparison, we consider a few other studies. Leahy, Muxlow & Stephens (1989) estimated the spectral indices of hot-spots between 151 and 1400 MHz, and found these to range from approximately -0.3 to -1.16 with a median value of approximately -0.8. Liu, Pooley & Riley (1992) estimated the injection spectral indices for a sample of 3CR FRII sources using flux density measurements between 38 MHz and $\sim$1 GHz, and found that these values range from -0.65 to -1, with a median value of -0.77. For a sample of giant radio sources, the injection spectral indices

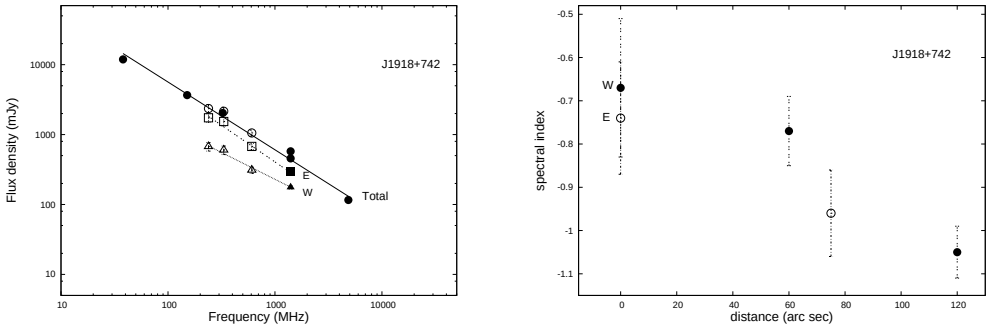

Figure 5. Left panel: the spectra of the J1918+742 and its components. The values have been taken from the following references: 38 MHz, Rees (1990); 151 MHz, Hales et al. (1991); 325 MHz, Westerbork Northern Sky Survey (WENSS) survey, Rengelink et al. 1997; 1400 MHz, NVSS survey; 1400 MHz, White & Becker (1992); 4850 MHz, Gregory & Condon (1991); 239, 332 and 607 MHz from this paper. Right panel: The spectral index profiles for the western and eastern components with an angular resolution of 45 arcsec using our measurements at 239, 332 and 607 MHz, and the NVSS image at 1400 MHz. For J1918+742 one arcsec corresponds to 3.190 kpc.

were found to be in the range of −0.55 to −0.88, with a median value of −0.6 (Konar et al. 2008; Jamrozy et al. 2008). However it is important to examine this further from observations at even lower frequencies by telescopes such as the LOw Frequency ARray (LOFAR).

High-frequency measurements are required to determine the break frequencies and spectral ages reliably. There is marginal evidence of spectral steepening in the lobes of J1211+743 from the 10500 MHz flux densities, but it would useful to confirm this from further observations at higher frequencies. The minimum energy magnetic field for the northern and southern lobes of J1211+743 are 0.15 and 0.14 nT respectively, yielding spectral ages of ∼30 Myr for a break frequency of ∼10 GHz. The minimum energy magnetic field of the jet is 0.19 nT which yields an age of $\lesssim$50 Myr for a break frequency $\gtrsim$5 GHz. The minimum energy magnetic field estimates of western and eastern lobes of J1918+742 are 0.16 and 0.20 nT respectively yielding ages of $\lesssim$70 Myr for break frequencies $\gtrsim$1.4 GHz.

6. Concluding remarks

Although models of evolution of jets in an initially asymmetric environment in the vicinity of the host galaxy lead us to expect that large radio sources should be reasonably symmetric in both flux density and separation of the oppositely-directed lobes from the parent galaxy (e.g. Jeyakumar et al. 2005), there are a number of highly asymmetric sources even on Mpc scales. These could be due to either environmental asymmetries on Mpc scales caused by the filaments, sheets and voids, or intrinsic asymmetries in the jets. Some, such as the ones studied here, namely J1211+743 and J1918+742, have a diffuse lobe without a significant hot-spot on one side of the parent galaxy, reminiscent of the lobes of FRI galaxies, and an edge-brightened lobe with a hot-spot on the

opposite side. J1211+743 has a prominent jet with the magnetic field lines following the bends in the jet, as seen in the FRII sources, but points in the direction of the diffuse lobe. This suggests that classification of hybrid morphology sources on the basis of a diffuse FRI-like lobe without a hot-spot may not be adequate. The asymmetries in brightness and structure of the oppositely-located components in these two large Mpc-scale sources are likely to be intrinsic rather than due to the effects of orientation and relativistic motion. The diffuse lobe facing the jet in J1211+743 could be due to a highly dissipative jet, as has been suggested earlier for several quasars without prominent hot-spots on the jet side.

The spectra of the lobes in J1211+743 and J1918+742 with a prominent peak or hot-spot tend to be flatter, and the spectral index appears to steepen with distance from the hot-spot, as has been seen earlier for most smaller-sized as well as giant radio sources. The variation of spectral index in the diffuse northern lobe of J1211+743 is small within ∼100 kpc of its outer edge, suggesting re-acceleration of particles. The integrated low-frequency spectral indices and also the values of α in the outer edges of the lobes are in the range of ~ -0.65 to -1.05, consistent with earlier low-frequency observations of luminous FRII radio sources. Observations at even lower frequencies by telescopes such as LOFAR, would be valuable to further probe the injection spectral indices and constrain particle acceleration models.

Acknowledgments

We thank Gopal-Krishna, Chiranjib Konar and Paul Wiita for their comments and suggestions on an early version of this manuscript, and Dave Green for very detailed comments on the present version of the manuscript. AP and SN thank NCRA, TIFR for hospitality during the course of this work, and Kumaon University, Nainital, for registering them as PhD students. AP is thankful to Jawaharlal Nehru Scholarship Ref: SU-A/287/2011-12/. AP, SN and MS are also thankful to DST, Government of India for financial support vide Grant No. SR/S2/HEP-17/2005. The GMRT is a national facility operated by the National Centre for Radio Astrophysics of the Tata Institute of Fundamental Research. We thank the staff for help during the observations. The National Radio Astronomy Observatory is a facility of the National Science Foundation operated under co-operative agreement by Associated Universities Inc. We are also thankful to the VLA staff for easy access to the archival data base. This research has made use of the NASA/IPAC extragalactic database (NED) which is operated by the Jet Propulsion Laboratory, Caltech, under contract with the National Aeronautics and Space Administration. We thank numerous contributors to the GNU/Linux group.

References

Baars J.W.M., Genzel R., Pauliny-Toth I.I.K., Witzel A. 1977, A&A, 61, 99
Barthel P.D., 1989, ApJ, 336, 606
Blandford R.D., Königl A., 1979, ApJ, 232, 34
Bridle A.H., Perley R.A., 1984, ARA&A, 22, 319

Condon J.J., Cotton W.D., Greisen E.W., Yin Q.F., Perley R.A., Taylor G.B. & Broderick J.J., 1998, AJ, 115, 1693
Dennett-Thorpe J., Bridle A.H., Scheuer P.A.G., Laing R.A., Leahy J.P., 1997, MNRAS, 289, 753
Dennett-Thorpe J., Bridle A.H., Laing R.A., Scheuer P.A.G., 1999, MNRAS, 304, 271
Fanaroff B.L., Riley J.M., 1974, MNRAS, 167, 31
Fanti C., et al., 1983, A&AS, 51, 179
Gaibler V., Khochfar S., Krause M., 2011, MNRAS, 411, 155
Garrington S.T., Leahy J.P., Conway R.G., Laing R.A., 1988, Nature, 331, 147
Garrington S.T., Conway R.G., Leahy J.P., 1991, MNRAS, 250, 171
Gilbert G.M., Riley J.M., Hardcastle M.J., Croston J.H., Pooley G.G., Alexander P., 2004, MNRAS, 351, 845
Gopal-Krishna, Wiita P.J., 2000, A&A, 363, 507
Gopal-Krishna, Wiita P.J., 2005, in Saha S.K., Rastogi V.K., eds, 21st Century Astrophysics, Anita Publications, New Delhi, p. 108 (arXiv:astro-ph/0409761)
Gopal-Krishna, Wiita P.J., Hooda J.S., 1996, A&A, 316, L13
Gregory P.C., Condon J.J., 1991, ApJS, 75, 1011
Hales S.E.G., Mayer C.J., Warner P.J., Baldwin J.E., 1991, MNRAS, 251, 46
Ishwara-Chandra C.H., Saikia D.J., 2000, MNRAS, 317, 658
Ishwara-Chandra C.H., Saikia D.J., McCarthy P.J., van Breugel W., 2001, MNRAS, 323, 460
Jägers W.J., 1986, Ph.D. Thesis, Leiden Univ. (Netherlands).
Jamrozy M., Konar C., Machalski J., Saikia D.J., 2008, MNRAS, 385, 1286
Jeyakumar S., Wiita P.J., Saikia D.J., Hooda J.S., 2005, A&A, 432, 823
Kapahi V.K., Saikia D.J., 1982, JApA, 3, 465
Konar C., Jamrozy M., Saikia D.J., Machalski J., 2008, MNRAS, 383, 525
Konar C., Hardcastle M.J., Croston J.H., Saikia D.J., 2009, MNRAS, 400, 480
Laing R.A., 1988, Nature, 331, 149
Laing R.A., Bridle A.H., Parma P., Murgia M., 2008, MNRAS, 391, 521
Laing R.A., Guidetti D., Bridle A.H., Parma P., Bondi M., 2011, MNRAS, in press
Lara L., Cotton W.D., Feretti L., Giovannini G., Marcaide J.M., Màrquez I., Venturi T., 2001a, A&A, 370, 409
Lara L., Màrquez I., Cotton W.D., Feretti L., Giovannini G., Marcaide J.M., Venturi T., 2001b, A&A, 378, 826
Leahy J.P., Muxlow T.W.B., Stephens P.W., 1989, MNRAS, 239, 401
Liu R., Pooley G., 1991a, MNRAS, 249, 343
Liu R., Pooley G., 1991b, MNRAS, 253, 669
Liu R., Pooley G., Riley J.M., 1992, MNRAS, 257, 545
Machalski J., Chyży K.T., Stawarz Ł., Kozieł D., 2007, A&A, 462, 43
McCarthy P.J., van Breugel W., Kapahi V.K., 1991, ApJ, 371, 478
Miley G.K., Osterbrock D.E., 1979, PASP, 91, 257
Mullin L.M., Riley J.M., Hardcastle M.J., 2008, MNRAS, 390, 595
Nandi S., Pirya A., Pal S., Konar C., Saikia D.J., Singh M., 2010, MNRAS, 404, 433
O'Dea C.P., Daly R.A., Kharb P., Freeman K.A., Baum S.A., 2009, A&A, 494, 471
Parma P., Murgia M., Morganti R., Capetti A., de Ruiter H.R., Fanti R., 1999, A&A, 344, 7

Pedelty J.A., Rudnick L., McCarthy P.J., Spinrad H., 1989, AJ, 97, 647
Rees N., 1990, MNRAS, 244, 233
Rengelink R.B., Tang Y., de Bruyn A.G., Miley G.K., Bremer M.N., Röttgering H.J.A., Bremer M.A.R., 1997, A&AS, 124, 259
Rudnick L., Owen F.N., 1977, AJ, 82, 1
Rudnick L., Edgar B.K., 1984, ApJ, 279, 74
Saikia D.J., 1984, MNRAS, 208, 231
Saikia D.J., Kulkarni V.K., 1994, MNRAS, 270, 897
Saikia D.J., Wiita P.J., 1982, MNRAS, 200, 83
Saikia D.J., Junor W., Muxlow T.W.B., Tzioumis A.K., 1989, Nature, 339, 286
Saikia D.J., Junor W., Cornwell T.J., Muxlow T.W.B., Shastri P., 1990, MNRAS, 245, 408
Saikia D.J., Jeyakumar S., Wiita P.J., Sanghera H.S., Spencer R.E., 1995, MNRAS, 276, 1215
Saikia D.J., Thomasson P., Jackson N., Salter C.J., Junor W., 1996, MNRAS, 282, 837
Saikia D.J., Jeyakumar S., Salter C.J., Thomasson P., Spencer R.E., Mantovani F., 2001., MNRAS, 321, 37
Scheuer P.A.G., 1995, MNRAS, 277, 331
Schoenmakers A.P., Mack K.-H., de Bryuyn A.G., Röttgering H.J.A., Klein U., van der Lann H., 2000, A&AS, 146, 293
Schoenmakers A.P., de Bruyn A.G., Röttgering H.J.A., van der Laan H., 2001, A&A, 374, 861
Subrahmanyan R., Saripalli L., Safouris V., Hunstead R.W., 2008 ApJ, 677, 63
Spergel D.N. et al., 2003, ApJS, 148, 175
Thomasson P., Saikia D.J., Muxlow T.W.B., 2003, MNRAS, 341, 91
Thomasson P., Saikia D.J., Muxlow T.W.B., 2006, MNRAS, 372, 1607
van Breugel W.J.M., Willis A.G., 1981, A&A, 96, 332
White R.L., Becker R.H., 1992, ApJS, 79, 331
Zhao J.-H., Burns J.O., Owen F.N., 1989, AJ, 98, 64